



Validation of Peregrine with Test Reactor Data

At the end of September, Pellet-Cladding Interaction (PCI) Challenge Problem Integrator Robert Montgomery reported that good progress has been made in demonstrating the Peregrine LWR fuel performance modeling software. The Peregrine fuel performance analysis computer program is being developed to provide a single rod 3-dimensional fuel performance modeling capability to assess safety margins and the impact of plant operation and fuel rod design on the thermo-mechanical behavior of nuclear fuel.

Peregrine is built using the Multiphysics Object Oriented Simulation Environment (MOOSE) computational framework architecture developed at Idaho National Laboratory, and uses the finite element method for geometric representation and a Jacobian-free, Newton-Krylov scheme to solve systems of partial differential equations. Peregrine also leverages key capabilities built into the Bison general purpose fuel modeling system. The ability to employ massively parallel computational capabilities is a key advantage to using Peregrine to study nuclear fuel performance, especially for multi-dimensional, multi-physics phenomena.

Many of the performance models used in Peregrine originated with EPRI's fuel performance code, Falcon. Falcon is an enhanced and integrated derivative of ESCORE and FREY, two historic EPRI codes developed in the 1980s with final release in 1990 and 1991 respectively. Enhancements (p.4)

About Tech Notes

CASL Tech Notes are produced by CASL's technical staff to spotlight areas of particular technical interest and to discuss CASL science and engineering innovation, accomplishments, activities, and plans. Tech Notes will be produced on a quarterly basis.

In this Issue...

- Validation of Peregrine with Test Reactor Data
- Effect of Grain Boundaries on Irradiation Growth of Zirconium-based Alloys
- Lift Forces in Bubbly Flows
- Implementing Integrated Steam Tables
- VERA Release Provided to RSICC for Future Release
- Initial VERA Neutronics/T-H/fuel Performance Coupling Demonstration
- Reflecting on the Past to Define CASL's Future
- EPRI Test Stand Launched

Effect of Grain Boundaries on Irradiation Growth of Zirconium-based Alloys

At the end of August, researchers S.I. Golubov, A.V. Barashev and R.E. Stoller delivered to CASL an analysis of the effect of grain size on the radiation growth of multi-grain, hexagonal close-packed (hcp) metals, taking into account the features of cascade damage due to neutron exposure. Irradiation growth occurs in zirconium-based alloys used for LWR fuel cladding. Experimental data suggests that irradiation growth deformation takes place via dislocation climb, formation of prismatic interstitial (and occasionally vacancy) dislocation loops, and vacancy loops on the basal planes.

In 2011, the ORNL-based team established a reaction-diffusion model for prediction of irradiation growth at an atomistic level, accounting for intra-cascade clustering of self-interstitial atoms (SIAs) with one-dimensional diffusion. The earlier model was useful in predicting the maximum possible strain rates due to irradiation growth, and provided insights into observations such as negative strain in the prismatic direction, co-existence of vacancy- and SIA-type prismatic loops, alignment of vacancy-type loops and voids along the basal planes, and also shed light on the role of cold work in radiation growth behavior. Building upon previously established models, the team has included considerations for polycrystalline materials and the absorption of mobile (p.6)

Lift Forces in Bubbly Flows

The dynamics of two-phase (gas/liquid) bubbly flows are complex: bubbles deform and disperse; large latent heats and heat capacity differentials influence local boiling; and relatively small changes in heated surface temperatures yield order of magnitude changes in boiling complexity. Because the local void volume has a direct feedback effect on reactor neutron flux and fuel rod power production, prediction of local boiling rates and bulk boiling effects in nuclear reactors is key in achieving a higher fidelity prediction of the fuel system temperature distribution, local and global power production, local fuel rod burnup, and CRUD deposition.

When the fuel rod surface temperature is high enough, steam bubbles nucleate and grow on the surface, detaching when the lift forces acting on the bubble are large (p.2)

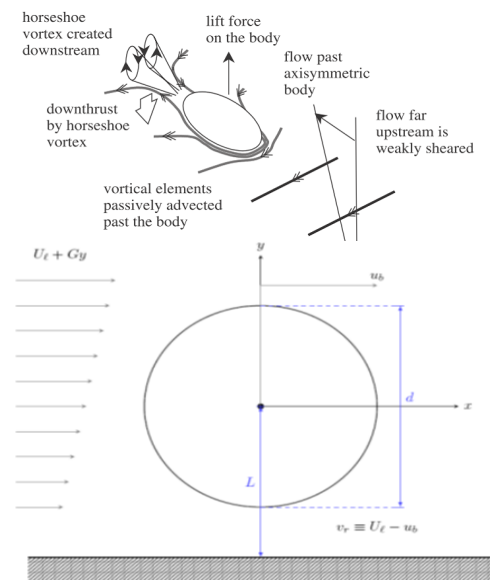


Figure 1 Illustration of Shear Flow around a Sphere

Lift Forces in Bubbly Flows. . . (continued from p. 1)

enough to overcome the suction force of the bubble on the rod. Shear lift forces are reaction forces that result as the flowing water passes over the surface of the bubble. They evolve as the shape and size of the bubble evolve and are also influenced by asymmetries in the upstream flow field.

Figure 1 provides a general illustration of a spherical bubble in flow. The general equation describing the forces acting on the bubble can be written as [1]:

$$\rho_b \left(\frac{4}{3} \pi a^3 \right) \frac{du_b}{dt} = F_I + F_A + F_L + F_D + F_B$$

Where F_I is the inertial force, F_A is the added mass term, F_L is the lift force, F_D is the drag force, F_B is the buoyancy force. When these terms are expanded, the resolved forces that are the target of the work are more easily identified:

$$\frac{du_b}{dt} = \frac{1 + C_M}{\gamma + C_M} \left(\frac{\partial v}{\partial t} + (v \cdot \nabla)v \right) + \frac{C_L}{\gamma + C_M} (v - u_b) \times \omega + \frac{1}{\gamma + C_M} \frac{3C_D}{8a} |v - u_b|(v - u_b) + \frac{\gamma - 1}{\gamma + C_M} g$$

Where u_b is the bubble velocity, v is the fluid velocity, C_M is the added mass coefficient, C_L is the lift coefficient, C_D is the drag coefficient, γ is the ratio of the densities (ρ_b/ρ), g denotes gravity and ω is vorticity.

In general, the coefficients are not constant, although their functional dependence has not been explicitly stated. A few effects have been left out, including those due to time history, density gradients, and temperature gradients. One of the lesser understood momentum closures is that due to the transverse forces. These transverse forces are very critical for LWR applications as transverse motion of bubbles in the narrow and long flow channels between the fuel rods can have a huge impact on the heat transfer and neutron moderation.

Many widely used two-fluid Computational Multiphase Fluid Dynamics (CMFD) codes, such as Ansys' CFX & Fluent, CD-adapco's Star-CCM+, and RPI's NPHASE-CMFD, implement Auton's shear lift model [5] and Antal's wall force model [7] as the two primary lift forces. All allow the user to tweak the model lift coefficients (C_L), although by default the coefficients are constants; some codes include alternative correlations for the lift coefficients. While the base form of the Auton lift force with a constant lift coefficient is an acceptable approximation at high Reynolds number (Re) and low Strouhal number (Sr) flows about roughly spherical bubbles, for different bubble shapes and orientations, the Auton closure should be modified. Additionally, Auton's model derivation assumes a Sr number of 1, and this assumption isn't always acceptable near the wall; when Sr is not small Auton's model overpredicts the shear lift force significantly. Substitute correlations presented in the past do include some bubble deformation and alternate orientations, but they don't appear to be sufficient for the range of PWR flow conditions.

Thus, for CASL, the immediate need from a CMFD perspec-

tive is to include the effect of the wall on shear lift forces. To address this need, ORNL researchers Thomas Daly and Sreekanth Pannala and UT-K professor Art Ruggles collaborated in developing a new closure for lift force that includes the wall effects. The team tested the closure using a comparison with fully developed turbulent pipe flow, and the new closure displays the correct asymptotic behavior.

Proposed CASL Closure Form

In order to accumulate a large body of data for use in constructing the new closure, the team first did a survey of existing work and extracted the information necessary to calculate the primary dimensionless parameters (see Table 1 for a listing; note that the characteristic length is the bubble diameter, d). The reference data and closures were plotted against the dimensionless parameters in Figure 6. As can be seen upon inspection of the plots, the existing closures do not capture the effect of all the different parameters and are limited in range. For example, Rastello's model [3, 4] is good at moderate to large Re and away from the wall, but is not as accurate at very low Re.

Using the referenced closures as the starting point, the research team worked to develop a new closure that could capture the empirically representative behavior of the lift coefficient versus Sr and Re. In order to better capture the influence of the wall, the proposed new closure includes an additional parameter, E , that renders the distance from the wall non-dimensional. The form was selected such that $E=1$ as the bubble touches the wall and approaches 0 as the bubble moves away from the wall. Eight different variations of the closure were investigated, with the best match (based on a least-squares approach), called "DRP," proposed for CASL adoption and future augmentation.

The new DRP lift closure was plotted with various independent parameters in Figures 6 and 7, and is shown with the reference data set.

The terms in the DRP lift closure that do not include the distance to the wall are based on Legendre & Magnaudet's model [2]. The new closure appears to capture both low and high Re behavior well. This was achieved by modifying Legendre's high Re model to allow for a local maximum near $Re = 50$. Like the other models it approaches the theoretical result of $C_L = 1/2$ as Re approaches infinity. Unlike the other models discussed in this report, the proposed model also includes a dependence on distance from the wall. This allows it to remain physically reasonable as a bubble approaches the wall.

Next steps

The correlation developed represents the initial formulation of the closure. Additional work is needed to provide a stronger theoretical footing and to include additional effects encountered in a PWR. The critical effects in increasing order of importance and difficulty that need to be accounted for (p.5)

Proposed CASL Closure Form for Bubbly Flow Lift Coefficients

$$J(Sr, Re) = \frac{2.255}{\left(1 + 0.2 \frac{Re}{Sr}\right)^{3/2}}$$

$$C_L^{low} = \frac{6J(Sr, Re)}{\pi^2 \sqrt{ReSr}} \quad C_L^{high} = \frac{1}{2} \left(\frac{1 + \frac{310}{Re} - \frac{242}{Re^2}}{1 + \frac{176}{Re} + \frac{566}{Re^2}} \right)$$

$$C_L^{nowall} = \left(C_L^{low2} + C_L^{high2} \right)^{1/2}$$

$$C_L = C_L^{nowall} \log_2 \left(\frac{E}{1-E} + 2 \right)^{-2.3}$$

Implementing Integrated Steam Tables

At the end of August, CASL published an equation of state model library for use with VERA. The IAPWS95 and IAPWS-IF97 standard models for the thermodynamic properties of water and the associated transport property models implemented within the library were verified to reproduce the analytic models across the range of validity. The performance of the interpolation package is over an order of magnitude faster than the analytic model equations, even for tables with very large numbers of nodes.

The International Association for the Properties of Water and Steam (IAPWS) has created and published multiple models for the thermodynamic and transport properties of water. The models are analytic formulas based upon polynomial expansions of free energies in density, temperature, and pressure. The many parameters of these expansions are calibrated to the various experimental measurements available for water and each are validated within their respective references. The models typically agree well with all the available data, except near the critical point.

The aim for CASL's implementation is to allow faster evaluation of properties. The IAPWS95 model equation uses density and temperature as independent variables. The IAPWS-IF97 contains five different equations that use a combination of density-temperature and pressure-temperature as independent variables. However, the current desired independent variable space for the solver is pressure and internal energy. In order to evaluate the steam properties using pressure and internal energy, the model equations must be inverted. The need for inversion is a key reason to tabulate the models, as the tabulation may be done directly in the desired pressure/internal energy space.

The standards documents define code verification tests for a subset of the thermodynamic and transport quantities, at a limited number of points in the domain of applicability of each region. These tests provided verification that the parameters of the basic polynomial equations are correctly entered and that the equations themselves are properly evaluated. The CASL implementation of the models have been tested successfully against these values and were found to be in good agreement in almost every case to the 9 decimal digits of accuracy reported in the documents. The next level of verification dealt with the consistency and accuracy of the variables that are not specified in the reference documents. In particular, the reference documents for IAPWS95 and IAPWS-IF97 report values for 5-6 thermodynamic quantities. However, CASL required computation and tabulation of a greater set of values (10-12). The last level of verification applied to the inversion algorithms.

The main goal of tabulation is to speed up the evaluation of state properties. This is accomplished through tabulation of the models directly into the desired pressure-internal energy phase space, avoiding multiple evaluations of the model polynomials. It is important, however, to verify that the tabulated properties still represent the analytic model. A new unstructured triangular (UTri) tabular format accomplishes these goals by allowing adaptation of the table grid so as to ensure a minimal amount of tabulated points that, when interpolated, reproduce the analytic models to within a certain error tolerance. Linear interpolation on the triangles provides for a very efficient computation. Efficient look up of thermodynamic states is accomplished through a tree structure that subdivides the phase space into regions containing roughly an equal number of triangles. Once a state is placed in one of these regions, the triangles contained therein are searched through using their barycentric coordinates to determine the triangle containing the interpolation point.

Construction of a table requires specification of the desired model, error tolerance, error sample size, independent variables, and table bounds. The table bounds are specified as a rectangular region in pressure/temperature space. This space is then warped into the desired space, as shown in Figure 2 at the highest energies. Thermal stability of the models ensure this mapping results in a valid boundary in the desired space. To simplify the triangle look up

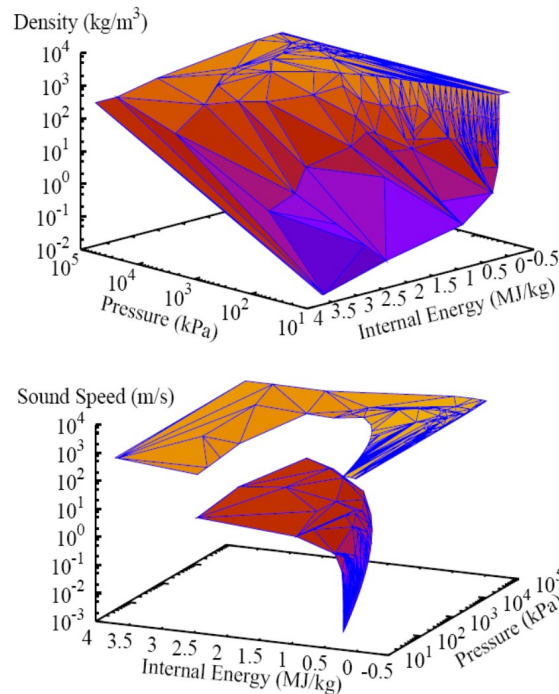


Figure 2 Interpolated density and sound speed with triangulation overlaid in blue for the IAPWS-IF97 model. Tabulation tolerance was 1.0 with 7 samples per triangle.

process, a rectangular space is regenerated by adding boundary triangles along the borders of the warped space. As these additional triangles lie flat along the boundary, interpolation points that fall in this region may be straightforwardly clipped to the pressure-temperature table bounds. Together the error tolerance and sample size define the verification level of the tabulation.

The tabulation process is accomplished through a table builder code. XML file format is used for the input, and an example is shown in Figure 3. In future, the steam table subroutine may be implemented within VERA modules that utilize steam tables to ensure consistent physical properties are used across the set of CASL codes.

Developers John Carpenter, Noel Belcourt, and Robert Nourgaliev noted that the table generator, model implementation, and interpolation package codes have been approved for release as open source software. They will be made available in future for download at <http://software.sandia.gov>.

For more information, see CASL-I-2013-0188-000.

```
<?xml version="1.0" encoding="UTF-8"?>
<EOSInference>
  <RunSettings model="water" tabulation="TRECT"/>
  <!-- Specification of the EOS model and its parameters -->
  <EOSModel>
    <water type="IAPWSIF97">
      <IParam name="TEMP_EXTRAP" value="1"/>
    </water>
  </EOSModel>
  <!-- Specification of the desired Tabulation -->
  <Tabulation A="18." Z="10.0" RRef="1." TRef="298." >
    <TRECT type="utri" basename="water" tolerance="1.0"
      boundarySamples="100" regionSamples="2"
      meshvars="PE" logvars="0" numthreads="8">
      <TBounds lower="273.16" upper="1073.15"/>
      <PBounds lower="1.e4" upper="1.e8"/>
    </TRECT>
  </Tabulation>
</EOSInference>
```

Figure 3 Example XML input to the steam table tabulation process

Validation of Peregrine with Test Reactor Data . . . (continued from p. 1)

continued from 1996 to 2004 when FALCON MOD01 Beta was released as the state-of-the-art LWR fuel performance code validated to high burn-up, capable of analyzing both steady state and transient fuel behavior. Falcon, now a brand name, is a result of further enhancements to make fuel performance analysis more accurate to nuclear utility fuel managers and reactor engineers.

Pellet-cladding mechanical interaction, or PCMI, refers to the contact between the fuel cladding and fuel pellet that is a normal part of fuel rod performance, typically occurring towards the end of the rod's first operational cycle. In the early 2000's several leaking rods were observed in LWRs and the root cause was found to be a combination of mechanical and chemical interactions between fuel pellets and fuel rod cladding, commonly called PCI. A necessary condition for these failures is contact between the pellet and cladding and a generated stress in the cladding caused by a power change.

PCI failures are often referred to as classical and non-classical type failures. Classical PCI failure refers to stress corrosion cracking (SCC) induced cladding fractures initiated during a power increase. Non-classical PCI failures can occur under less severe operating conditions where other factors, such as a missing pellet surface, overstress the cladding. PCI failures may occur in both PWRs and BWRs. The failure mechanism is more prevalent in BWRs because control rod movements are more frequent. In PWRs, reactor power is typically controlled through the addition of soluble boron in the coolant, and consequently PCI failures are less frequent. However, during reactor power increases, and specifically during a class II transient (anticipated operational occurrence), PCI failures may occur in a PWR.

Thus, to reliably predict PCI failures, the code must be capable of describing the thermal, mechanical, and chemical properties and constitutive relationships of both pellet and cladding as functions of temperature, chemistry, burnup, fission density, fast flux, fast fluence, and many other state variables.

The non-linear fuel rod behavior resulting from the interactions of these properties require key assumptions concerning material dependencies, numerical formulations, and geometric representation to satisfy runtime, numerical convergence, and assumption limitations, giving rise to simplifications in the approaches to de-emphasize one phenomenon over others. Consequently, fuel performance modeling software requires extensive verification, calibration, and validation exercises to demonstrate their ability to accurately represent nuclear fuel behavior.

The current validation work is based on fourteen fuel rods irradiated in a variety of commercial and test reactors to assess the fuel temperature, cladding deformation, and fission gas release modeling capabilities. These 14 fuel rods experienced irradiation conditions representative of beginning of life all the way to high burnup. Because of the nature of the irradiation programs, these fuel rods were modeled using axis-symmetric geometric representations of the cylindrical fuel pellet column and cladding as shown in Figure 4. A comparison of Peregrine to fuel centerline temperatures from more than 550 measurements is shown in Figure 5, along with a comparison to the

industry fuel performance modeling software package, Falcon.

The validation activities provide confidence in the development of Peregrine to date, but also highlight the challenges in accurately modeling the complex thermal and mechanical behavior inherent in nuclear fuel performance. A number of improvements in the material and behavior models have been identified by the development team, and future development activities will focus on enhancing and implementing these models into Peregrine. In particular, improvements to the representation of pellet cracking and relocation, fission gas retention and release, gap thermal conductance, pellet-clad mechanical contact (including improved advanced creep and growth models) and cladding oxidation and hydride formation and growth are needed. These advancements will expand the fidelity of Peregrine and provide the ability to accurately model three-dimensional aspects of fuel performance, such as pellet-clad interaction with missing pellet surfaces. In some cases, advanced models for these topics are being developed within the Materials Performance and Optimization (MPO) focus area and will be implemented in Peregrine to enhance code capability.

For more information, see CASL-I-2013-0122-000 and CASL-I-2013-0165-000.

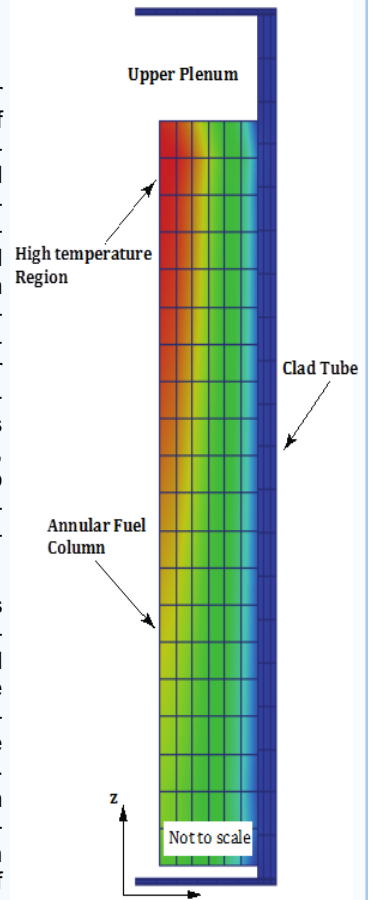


Figure 4 fuel rods were modeled using axis-symmetric geometric representations of the cylindrical fuel pellet column and cladding.

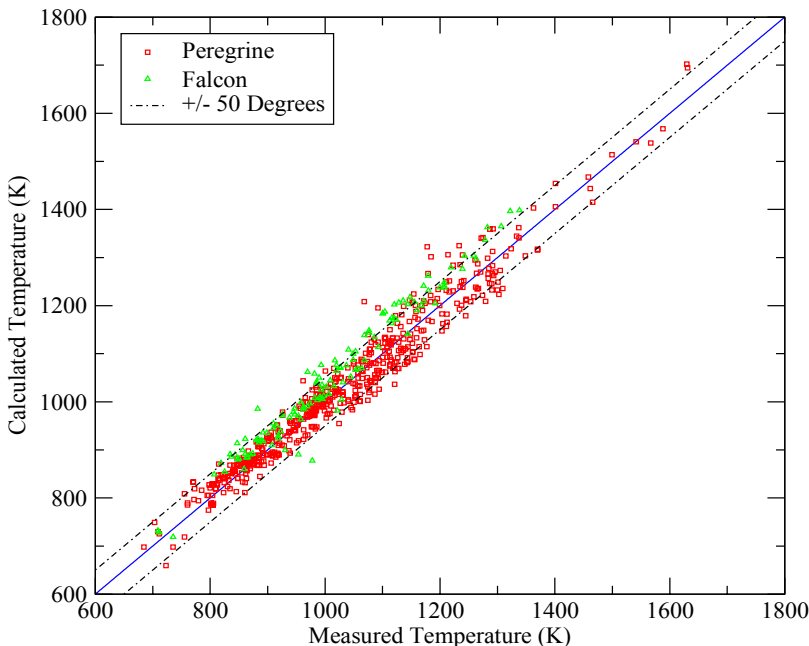


Figure 5 Comparison of Falcon-calculated and Peregrine-calculated fuel centerline temperatures for 550 experimentally measured observations.

Lift Forces in Bubbly Flows. . .

(continued from p. 2)

in two-phase PWR conditions are:

- ◆ Blockage (reduced area on the side of the wall for flow)
- ◆ No-slip condition and the resulting velocity/vorticity profile
- ◆ Turbulence (especially for small bubbles when fluctuations can influence bubble transport)
- ◆ Deformation (for large bubbles)
- ◆ Swarming (high bubble density, polydispersity, break-up and coalescence)
- ◆ Boiling effects.

For more information, see CASL-I-2013-0143-000.

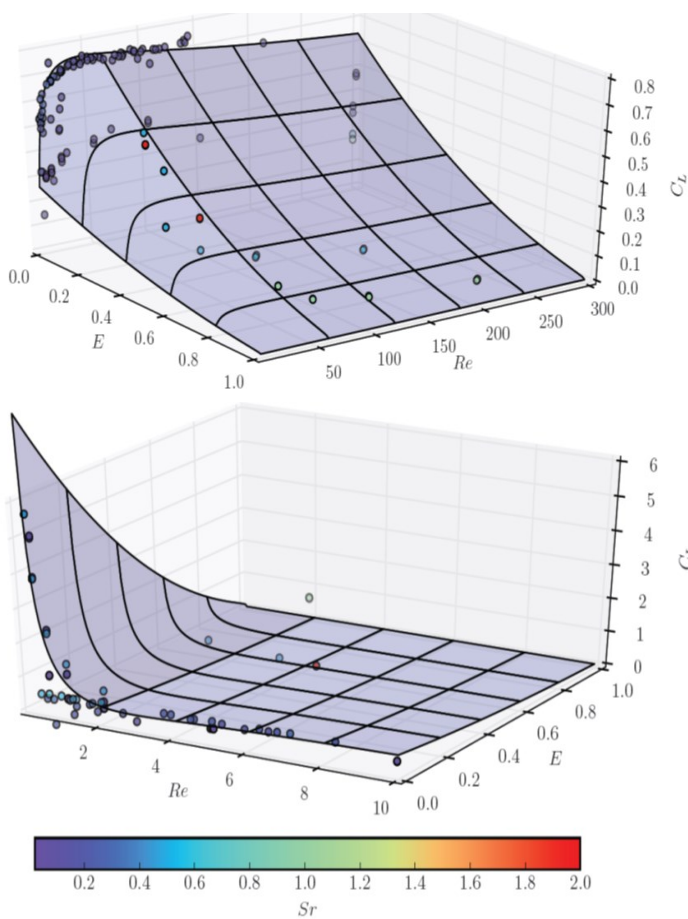


Figure 7 Surface Plot of DRP model and pointwise data for $Re > 2$ (top) and $Re < 2$ (bottom)

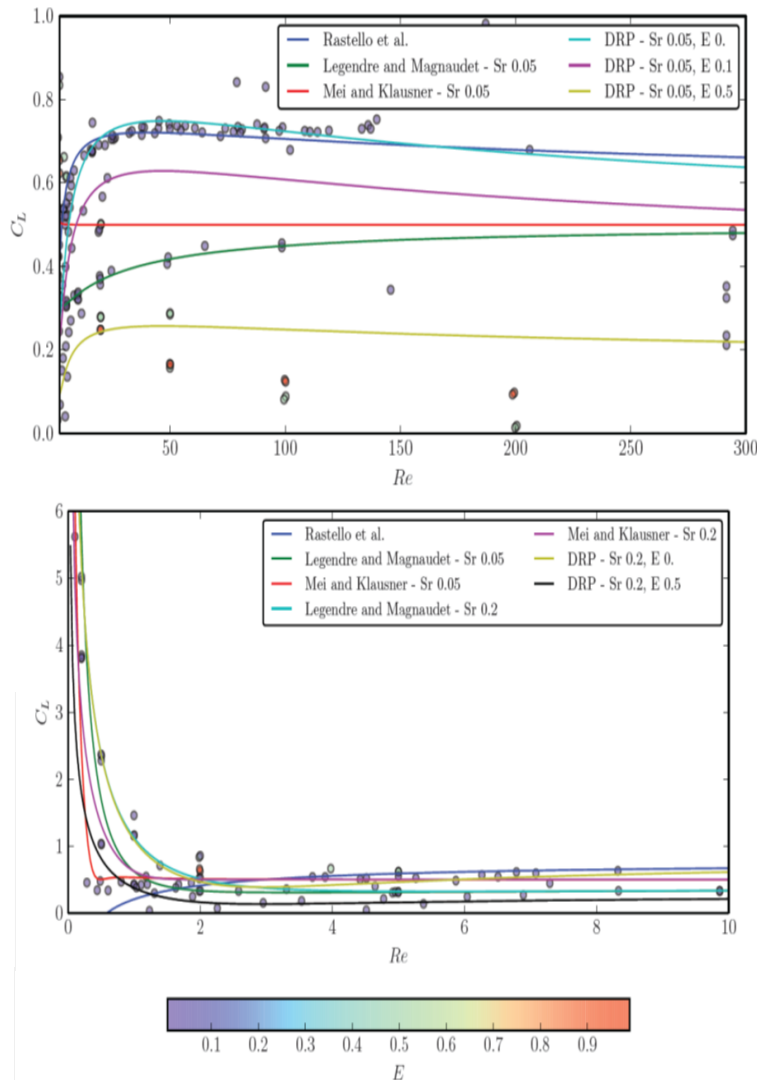


Figure 6 DRP Lift Coefficient for $Re > 10$ (top) and $Re < 10$ (bottom) plotted with reference closures

Table 1 Dimensionless Parameters

Name and Definition	Description
$Re = \frac{dv_r}{\nu}$	Particle Reynolds Number
$Sr = \frac{dG}{v_r}$	Dimensionless shear
$E = \frac{d}{2L}$	Dimensionless distance from wall
$C_L = \frac{F_L}{\frac{\rho\pi}{6}d^3v_rG} = \frac{F_L}{\frac{\rho\pi}{6}v^2Re^2Sr}$	Auton lift Coefficient [7]
$C_L^{Drag} = \frac{F_L}{\frac{\rho\pi}{8}d^2v_r^2} = \frac{F_L}{\frac{\rho\pi}{8}v^2Re^2}$	Drag law type lift coefficient

Several works are referenced in the full CASL report; those works referred to in this article include:

- [1] J. Magnaudet and I. Eames. "The motion of high-Reynolds-number bubbles in inhomogeneous flows." *Annual Review of Fluid Mechanics*, 32(1): 659-708, 2000.
- [2] D. Legendre and J. Magnaudet. "The lift force on a spherical bubble in a viscous linear shear flow." *Journal of Fluid Mechanics*, 368:81-126, 1998.
- [3] M. Rastello, J.L. Marie, and M. Lance. "Drag and lift forces on clean spherical and ellipsoidal bubbles in a solid-body rotating flow." *Journal of Fluid Mechanics*, 682(1):434-459, 2011.
- [4] M. Rastello, J.L. Marie, N. Grosjean, and M. Lance. "Drag and lift forces on interface-contaminated bubbles spinning in a rotating flow." *Journal of Fluid Mechanics*, 624(1):159-178, 2009.
- [5] R. Mei and JF Klausner. "Shear lift force on spherical bubbles." *International Journal of Heat and Fluid Flow*, 15(1):62-65, 1994.
- [6] Ernst A Van Nierop, Stefan Luther, Johanna J Bluemink, Jacques Magnaudet, Andrea Prosperetti, and Detlef Lohse. "Drag and lift forces on bubbles in a rotating flow." *Journal of Fluid Mechanics*, 571(1):439-454, 2007.
- [7] S. Antal, R. Lahey, and J. Flaherty. "Analysis of phase distribution in fully developed laminar bubbly two-phase flow." *International Journal of Multiphase Flow*, vol. 17, no. 5, pp 635-652, 1991.

Effect of grain boundaries. (continued from p. 1)

defects by grain boundaries. The work illustrates the relationship between grain shape, grain size, dislocation density and radiation growth through demonstrations of three types of grains: a spherical grain, an elongated grain, and a flat grain.

In a general case, the sink strength of grain boundaries oriented in x,y and z directions can be approximated as:

$$k_g^2 = k_{gx}^2 + k_{gy}^2 + k_{gz}^2 \approx 5 \left[\frac{\alpha_{gx}}{R_g^2} + \frac{\alpha_{gy}}{R_g^2} + \frac{\alpha_{gz}}{R_g^2} \right],$$

where:

$$\alpha_{gi} = \frac{3\varepsilon_{gi}^2 [\varepsilon_{gi} \coth(\varepsilon_{gi}) - 1]}{\varepsilon_{gi}^2 - 3 [\varepsilon_{gi} \coth(\varepsilon_{gi}) - 1]}, \quad i = x, y, z,$$

$$\varepsilon_{gi} = R_{gi} \sqrt{\rho}.$$

and:

k_g is the grain boundary sink strength,
 R_g is the grain radius,
 ρ is the total dislocation density, and
 ε_{gi} is SIA fraction clustered in cascades.

In the case of a spherical grain,

$R_{gx} = R_{gy} = R_{gz} = R_g$, and the strain equations are given by:

$$\frac{d\varepsilon_x^{tot}}{d\phi} = \chi \left(\frac{1}{2} - \frac{\rho_x R_g^2 + 5}{\rho R_g^2 + 15} \right),$$

$$\frac{d\varepsilon_y^{tot}}{d\phi} = \chi \left(\frac{1}{2} - \frac{\rho_y R_g^2 + 5}{\rho R_g^2 + 15} \right),$$

$$\frac{d\varepsilon_z^{tot}}{d\phi} = -\chi \frac{\rho_z R_g^2 + 5}{\rho R_g^2 + 15},$$

As illustrated in Figure 8a, strain increases as grain size decreases. Thus, if the grain size is large enough, the radiation growth induced strain is the same as that for a single crystal. For low dislocation density, the effect of grain boundaries is visible at a grain radius of ~6 mm. When there is a high density of dislocations the effect is important at grain radii of ~1mm. In the case of very small grains ($\rho_{x,y,z} R_g^2 \ll 5$), the strain rates can reach quite large values on the order of $5 \times 10^{-3} \text{ dpa}^{-1}$ independent of the magnitude of dislocation densities.

For the case where the grains are elongated such that $R_{gx} \ll R_{gy}, R_{gz}$:

$$\frac{d\varepsilon_x^{tot}}{d\phi} = \chi \left(-\frac{1}{2} + \frac{1}{5} (\rho_y + \rho_z) R_{gx}^2 \right),$$

$$\frac{d\varepsilon_y^{tot}}{d\phi} \approx \chi \left(\frac{1}{2} - \frac{1}{5} \rho_y R_{gx}^2 \right),$$

$$\frac{d\varepsilon_z^{tot}}{d\phi} \approx -\frac{1}{5} \chi \rho_z R_{gx}^2.$$

As illustrated in Figure 8b, for the non-basal elongated case, the strain rate in the prismatic direction reaches a maximum value of $\chi/2$, which is about $10^{-2}/\text{dpa}$, negative in the x-direction and positive in y, whereas it is practically zero in the basal direction.

The situation is quite different in the case when a grain is elongated in a way that it has a small size in the basal direction, i.e. that $R_{gz} \ll R_{gx}, R_{gy}$:

$$\frac{d\varepsilon_x^{tot}}{d\phi} = \chi \left(\frac{1}{2} - \frac{\rho_x R_{gz}^2}{5} \right) \approx \frac{\chi}{2},$$

$$\frac{d\varepsilon_y^{tot}}{d\phi} = \chi \left(\frac{1}{2} - \frac{\rho_y R_{gz}^2}{5} \right) \approx \frac{\chi}{2},$$

$$\frac{d\varepsilon_z^{tot}}{d\phi} = -\chi \frac{\rho_z R_{gz}^2 + 5}{\rho R_{gz}^2 + 5} = -\chi \left(1 - \frac{(\rho - \rho_z) R_{gz}^2}{5} \right) \approx -\chi.$$

In this case the strain rates in the prismatic directions also reach the maximum value of $\chi/2$; however, both of them are positive. In addition, the strain rate in the basal direction is also reaches the maximum negative value of χ . The results of this case are illustrated in Figure 8c.

Finally, the case where the grains are very flat ($R_{gx} = R_{gy} = R_o \ll R_{gz}$):

$$\frac{d\varepsilon_x^{tot}}{d\phi} = \chi \left(-\frac{1}{2} + \frac{1}{5} (\rho_y + \rho_z) R_{gx}^2 \right) \approx -\frac{\chi}{2},$$

$$\frac{d\varepsilon_y^{tot}}{d\phi} \approx \chi \left(\frac{1}{2} - \frac{1}{5} \rho_y R_{gx}^2 \right) \approx \frac{\chi}{2},$$

$$\frac{d\varepsilon_z^{tot}}{d\phi} \approx -\frac{1}{5} \chi \rho_z R_{gx}^2 \approx 0.$$

As shown in Figure 8d, the largest positive (p.9) and negative strain rates are similar in magnitude and are significantly smaller than the other cases.

These models are planned for future integration to the VPSC multigrain atomistic material models being developed by LANL for implementation by CASL for use in prediction of cladding deformation. For more information, see CASL-I-2013-0182-001-a / ORNL/LTR-2013/340 and the following reference works:

- [8] R.A. Holt, J. Nucl. Mater., In-reactor deformation of cold-worked Zr-2.5Nb pressure tubes 372 (2008) 182.
- [9] S.I. Golubov, A.V. Barashev, R.E. Stoller, On the origin of radiation growth of hcp crystals, ORNL/TM-2011/473.
- [10] Singh B.N., Eldrup M., Zinkle S.J., Golubov S.I., On Grain Size Dependent Void Formation in Copper Irradiated with Fission Neutrons, Philos. Mag. Series A. 82, No. 6 (2002) 1137-11-58.

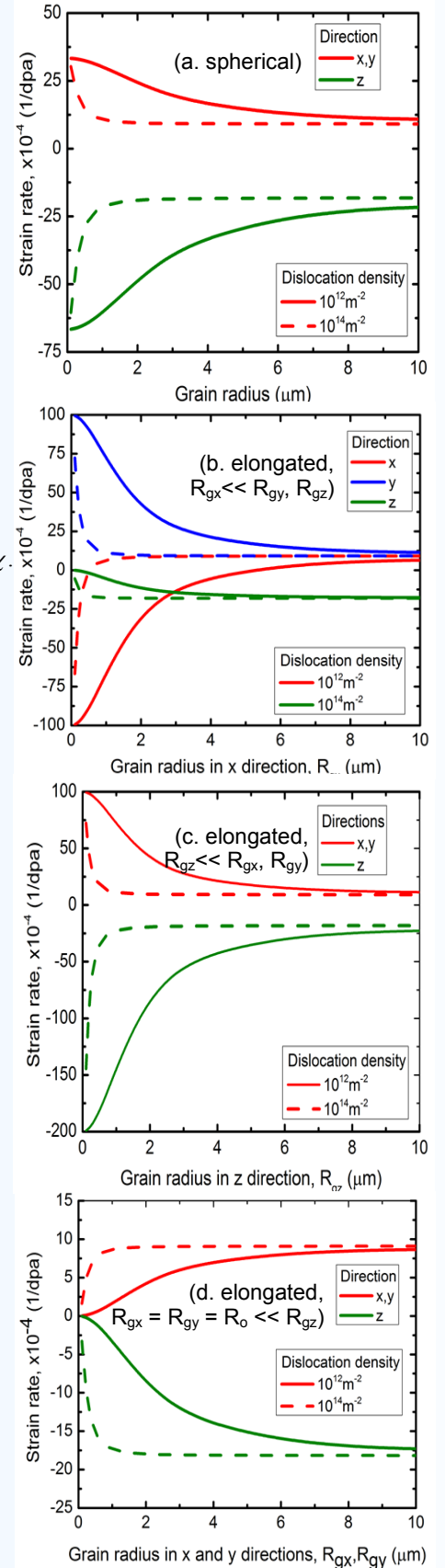


Figure 8 Calculated strain rates for various postulated grain aspect ratios for uniform distribution of prismatic dislocations (ρ) and $\varepsilon=0.02$. (a) spherical; (b) elongated in one prismatic direction; (c) elongated in both prismatic directions; (d) elongated in the basal direction.

VERA Update Provided to RSICC for Future Release

At the end of September, CASL prepared a release of key VERA components that will be distributed by the ORNL *Radiation Safety Information Computational Center (RSICC)*. The release represents a major step towards large-scale deployment of the VERA capabilities. This release is intended for evaluation and testing and will be provided to test users with a goal of providing early access to VERA while providing feedback to CASL. Expected target organizations for the extended testing include CASL Industry Council members, independent software vendors (to preview the software in support of interoperability objectives), U.S. universities and national labs (for research purposes), and other industry users (for early evaluation). The update is currently undergoing review and finalization and is expected to be released by the end of December 2013.

One goal of the recent update was to further exercise and refine CASL's release process, which includes formal review steps for component inclusion in the release. For the latest update, a final readiness review was held on September 30, 2013 with PHI and AMA confirming all release requirements had been met. CASL Quality Assurance Manager, Matt Sieger, stated that "the release process gives us a repeatable framework for the necessary quality assurance and other activities such as documentation updates, intellectual property, and export control reviews before a release to external (non-CASL) users is completed. The readiness reviews were very helpful in driving preparations for the release, and an after-action review meeting was held to examine the process, document lessons learned, and identify things we want to improve for the next release."

The test releases are necessary precursors to broader re-

leases to provide a robust release process. Future work that must be completed prior to a release includes finalization of the release licenses, streamlining the export control reviews, and improvements in VERA documentation, including component theory, user/input manuals, and installation guide. This test and evaluation release contains an initial subset of VERA physics and infrastructure components shown in Table 2. Those codes not selected for inclusion in this release will be considered in a future update.

Table 2 VERA components included in September RSICC release

Component	Included	Not Included	Comments
<i>Physics Components</i>			
COBRA-TF	X		Standalone with VERAIn input.
Insilico	X		Sn/Spn with Scale/XSProc and VERAIn input
Coupled Insilico + COBRA-TF	X		Single assembly
Hydra-TH		X	
MPACT	X		Lattice physics, no 3D
MAMBA-2D		X	
Peregrine		X	
MOOSE/Bison		X	
Tiamat (CTF + Insilico + Peregrine)		X	
Coupled COBRA-TF + MAMBA-2D		X	
Shift		X	
<i>Infrastructure Components and TPLs</i>			
Trillinos	X		
TriBITS	X		
VERAIn	X		Common VERA input parser
Dakota	X		
LIME	X		
DataTransferKit	X		
Other Required TPLs		X	Instructions on how to obtain TPLs will be provided in the VERA Installation Guide.

Initial VERA Neutronics/T-H/Fuel Performance Coupling Demonstration

At the end of July, CASL completed an initial capability demonstration with the coupled neutronics, channel flow and rod performance codes. The cross-cutting team of researchers included Roscoe Bartlett (ORNL), Kenneth (Noel) Belcourt (SNL), Kevin Clarno (ORNL), Greg Davidson (ORNL), Tom Evans (ORNL), Derek Gaston (INL), Jason Hales (INL), Russell Hooper (SNL), Wenfeng Liu (ANATECH), Robert Montgomery (PNNL), Scott Palmtag (Core Physics Inc), Roger Pawlowski (SNL, Milestone Lead), Robert Salko (ORNL), Rod Schmidt (SNL), Dion Sunderland (ANATECH) and John Turner (ORNL). The example problem, run with the coupled physics suite (code named "Tiamat" by the team), was a 17x17 fuel assembly at hot full power conditions.

In the initial application, three physics codes were coupled together: Insilico (neutronics), COBRA-TF (T-H), and Peregrine (fuel performance). As illustrated in Figure 9, two-way coupling was implemented on the multiple parameters being exchanged. Five data transfer objects were implemented for this capability, and all data transfers had to account for parallel communication patterns, unit conversions, pin axis orientation and active fuel offset height. The Data Transfer Kit (DTK) was used for determining the parallel communication

mappings and for moving all data between codes.

The different physics associated with the codes are strongly coupled and nonlinear, meaning that the quantities calculated in each physics component and passed to the other have a significant impact on the physical quantities computed in the other physics components. To solve the coupled system, a simple block-Jacobi fixed-point (FP) iteration used. In this method, each code is solved concurrently in its own MPI process space using data from the other coupled codes at the previous iteration. An advantage of this scheme is that if the codes are load balanced, each can run in its own process space at the same time, maximizing the process utilization. Separating each component into its own MPI process space also helps to mitigate potential memory issues. The design allows switching between both Jacobi and Gauss-Seidel algorithms. This milestone has also developed tools to assist in splitting applications into unique MPI process spaces.

The demonstration was successful, providing a fully converged, multiphysics solution. Development will continue in FY2014 with refinements

to load balancing and data transfers, along with several other team-recommended improvements.

For more information, see CASL-I-2013-0165-000.

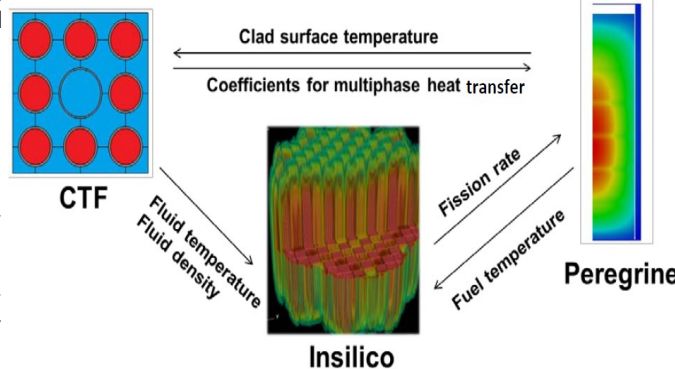


Figure 9 Graphical depiction of coupled physics data transfers



CASL's Chief Scientist, Paul Turinsky

Reflecting on CASL's Past to Define it's Future

These past few months, I've spent a lot of time considering the opportunities for extending CASL's codes and applications. CASL passed the 3-year mark in July, and it seems appropriate to reflect on what we've accomplished to date, as we define what CASL will accomplish in the next 24 months, and what it might do with a 5-year extension.

CASL's first 2-years of work were heavily focused on developing the foundational physics of the ModSim capabilities. We spent many hours building

commercial reactor-aware capabilities into the higher fidelity generalized neutronics, fluid flow, and rod performance physics codes. We also worked very hard at developing many micro-scale models to develop additional higher fidelity options.

In Year 3, many of the foundational physics capabilities were still under active development, but had reached a maturity level sufficient for collection and coupling under the VERA infrastructure. Also, early in Year 3, the Challenge Problem Integrators were instituted to create detailed implementation plans aimed at sharpening our development focus and ensuring complete lifecycle simulation capabilities. We also made major progress on VERA deployment through the launch of the Westinghouse AP1000 Test Stand.

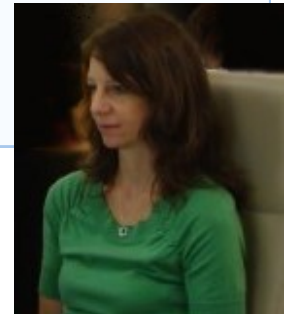
In these two final years of our initial funding, we hope to launch several more test stands: EPRI's fuel performance-focused test stand has already begun; the TVA lower plenum flow anomaly test stand is planned to start this winter; and several Industry

Council-proposed test stands are under discussion. The micro-scale R&D work is expected to have matured enough for integration with the physics models and closure relationships currently being utilized, and the remaining integration of capabilities and coupling under the VERA infrastructure should support simulation capabilities for the CASL Challenge Problems.

Not everything has gone as planned. We underestimated the effort required in CFD, more than once assumed existing code capabilities would be adequate with minor reconfigurations to later determine otherwise, and pursued ModSim paths where the computational requirements proved to exceed those likely to be acquired by industry. These lessons were difficult for the team, but we have learned from them and will do our best not to repeat them.

The remaining 24 months of our initial funding will certainly be challenging, with the many physics capabilities coming together under a single VERA architecture for coupled, converged solutions. But at the end of this long road we will have achieved the basis of a very powerful toolset that not only supports solutions to CASL's established Challenge Problems, but also has the potential to uncover issues before they play out in our reactors.

If fortunate enough to be awarded a second 5-years of funding, this will provide CASL the opportunity to not only further improve on the ModSim capabilities that have been developed, but to expand capabilities to address other Challenge Problems and to move beyond the current focus on Generation II and III PWRs to other vintages and types of LWRs.



Industry Council Chairman and EPRI Test Stand Lead, Heather Feldman (EPRI)

EPRI Test Stand Launched

In FY13, CASL launched a series of test stands aimed at implementing VERA in industrial settings to solve industrial problems. The test stands are integral to CASL's long-term goal of producing tools that can be used to inform industry decisions regarding extending the life of existing commercial power reactors. The first test stand, hosted by Westinghouse was launched in FY2013 and focused on CASL neutronics tools. The EPRI-sponsored test stand will utilize the Peregrine fuel performance tool and

COBRA-TF channel flow capability to simulate duty-related fuel rod behavior for critical pins in selected 17x17 PWR fuel assemblies in a selected Watts Bar cycle.



EPRI Fuel Reliability Program (FRP) Project Manager Martin Pytel

EPRI Fuel Reliability Program (FRP) Project Manager Martin Pytel will adopt a three-stage approach to the simulation: first, a quarter-core model will be used to screen for bounding fuel assemblies using VERA-CS with its simplified Cobra-TF fuel rod models; next, the as-

semblies will be modeled to look for bounding fuel rods using Peregrine's 2D axis-symmetric capability; and finally, local effects modeling to determine margin to duty-related failure will be completed with Peregrine 3D.

EPRI installed VERA on their new computer cluster, Phoebe, in October. The deployment included the latest VERA-CS and Peregrine, as well as necessary infrastructure tools (e.g., Trilinos, TriBITS, VERAIn, Dakota, LIME, DataTransferKit, MOOSE). EPRI's test stand project lead, Heather Feldman, noted "EPRI is looking forward to putting VERA through the paces to test the existing capa-

bilities on an industry fuel performance problem. We'll become familiar with the software and CASL will get early feedback from an end user. Both organizations benefit." The codes and documentation on the EPRI test stand will be updated periodically to ensure that the latest capabilities are in place.

About CASL

CASL is a DOE Energy Innovation Hub focused on modeling & simulation of Commercial Light Water Reactors. CASL connects fundamental research and technology development through an integrated partnership of government, academia and industry that extends across the nuclear energy enterprise. Learn more at www.casl.gov.



U.S. DEPARTMENT OF ENERGY
ENERGY
Nuclear Energy

Acknowledgments

This document is sponsored by the U.S. Government under contract DE-AC05-00OR22725 with UT-Battelle, LLC, which manages the Oak Ridge National Laboratory (ORNL). Accordingly, the U.S. Government retains a nonexclusive, royalty-free license to publish or reproduce these documents, or to allow others to do so, for U.S. Government purposes. Unless otherwise noted, they have been placed in the public domain, although we request the following credit line be used when documents reproduced elsewhere: "Courtesy of CASL, Oak Ridge National Laboratory, U.S. Dept. of Energy."

Disclaimer

This document was prepared as an account of work sponsored by an agency of the U.S. Government. Neither the U.S. Government nor any agency thereof, or any of their employees, makes any warranty, express or implied, or assumes any legal liability or responsibility for the accuracy, completeness, or usefulness of any information, apparatus, product, or process disclosed, or represents that its use would not infringe privately owned rights. Further, ORNL is not responsible for the contents of any off-site pages referenced. Reference to any specific commercial product, process, or service by trade name, trademark, manufacturer, or otherwise does not necessarily constitute or imply its endorsement, recommendation, or favoring by the U.S. Government or any agency thereof. The views and opinions of document authors do not necessarily state or reflect those of the U.S. Government or any agency thereof.

Contact Us:

Technical Editor	Rose Montgomery	Oak Ridge National Laboratory
Distribution	Linda Weltman	PO Box 2008, MS6003
Email	casl-info@casl.gov	Oak Ridge, TN 37831-6003

OAK RIDGE NATIONAL LABORATORY

MANAGED BY UT-BATTELLE FOR THE DEPARTMENT OF ENERGY